ACS Photonics

Article

pubs.acs.org/journal/apchd5

Transfer-Printing of Tunable Porous Silicon Microcavities with Embedded Emitters

Hailong Ning,[†,⊥] Neil A. Krueger,[†,⊥] Xing Sheng,[†] Hohyun Keum,[‡] Chen Zhang,[§] Kent D. Choquette,[§] Xiuling Li,[§] Seok Kim,[‡] John A. Rogers,[†] and Paul V. Braun*[,†]

[†]Department of Materials Science and Engineering, [‡]Department of Mechanical Science and Engineering, and [§]Department of Electrical and Computer Engineering, University of Illinois at Urbana−Champaign, Urbana, Illinois 61801, United States

Supporting Information

ABSTRACT: Here we demonstrate, via a modified transfer-printing technique, that electrochemically fabricated porous silicon (PSi) distributed Bragg reflectors (DBRs) can serve as the basis of high-quality hybrid microcavities compatible with most forms of photoemitters. Vertical microcavities consisting of an emitter layer sandwiched between 11- and 15-period PSi DBRs were constructed. The emitter layer included a polymer doped with PbS quantum dots, as well as a heterogeneous GaAs thin film. In this structure, the PbS emission was significantly redistributed to a 2.1 nm full-width at half-maximum around 1198 nm, while the PSi/GaAs hybrid microcavity emitted at 902 nm with a sub-nanometer full-width at half-maximum and quality-factor of 1058. Modification of PSi DBRs to include a PSi cavity coupling layer enabled tuning of the total cavity optical thickness. Infiltration of the PSi with Al_2O_3 by atomic layer deposition globally red-shifted the emission peak of PbS quantum dots up to ∼18 nm (∼0.9 nm per cycle), while introducing a cavity coupling layer with a gradient optical thickness spatially modulated the cavity resonance of the PSi/GaAs hybrid such that there was an ∼30 nm spectral variation in the emission of separate GaAs modules printed ∼3 mm apart.

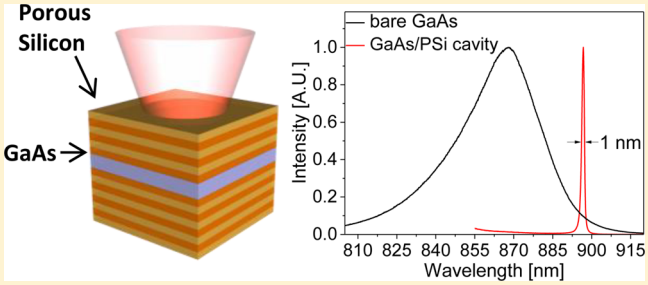

KEYWORDS: *silicon photonics, vertical cavity emitter, silicon/III−V hybrid, gradient refractive index, distributed Bragg reflector*

Porous silicon (PSi) is formed by electrochemically etching silicon in a hydrofluoric acid-based electrolyte, with the resultant porosity (i.e., void fraction) determined by the applied current density, etch solution chemistry, and silicon doping.[1] This material first drew considerable attention for its visible photoluminescence at room temperature,[2,3] leading to consideration of Si-based light sources for optoelectronics.[4,5] But, the research that followed was unable to advance PSi light-emitting technology to a level of performance meriting widespread implementation. PSi was, however, found to be a very versatile optical material, in particular for sensing applications,[6−8] because its effective refractive index, and thus optical properties, can be modulated by foreign materials that enter the porous network.[9−11] Porosity variations induced by time-varying etching currents enable the formation of high-quality superlattices[12] with pronounced optical signatures, including high quality-factor (*Q*-factor) microcavities[13,14] with the potential to function as resonant cavities for lasers.[15]

The versatility and optical properties of PSi microcavities, coupled with highly efficient emitters, may provide a new platform for realizing the strong light emission manipulation required for lasers,[16] displays,[17] and quantum information processing.[18,19] However, to date, emission modification efforts using PSi microcavities have relied heavily on the limited scope of emitters that can be either embedded into the mesoporous structure[20−25] or implanted into the Si wafer used to fabricate the PSi.[26] While these efforts have showed promise, lack of spatial control of the emitter distribution may lead to fluorescence quenching due to energy transfer among the emitters or between the emitters and the PSi surface.[27−29] Fabrication of hybrid structures composed of a well-defined, high-quality emitting cavity layer introduced between PSi distributed Bragg reflectors (DBRs) can address the above issues, potentially bridging the gap between PSi photonics and optoelectronic devices. Prior to the work here, realization of PSi hybrid microcavities has been hindered by difficulties in transferring fragile PSi films from a donor substrate to an acceptor substrate without damage. Methods of assembling PSi photonic devices have been proposed, including dry-removal lithography[30] and biofunctionalization-driven self-assembly.[31] However, these techniques have been geared toward the formation of PSi-based sensing arrays that lack the optical properties required for emission modification.[32,33] Recently, approaches based on transfer-printing have successfully enabled a broad variety of heterogeneously integrated optoelectronic and photonic systems.[34−37] In these methods, the kinetically controlled adhesion between the elastomeric stamp and the object to be transferred allows for high-quality assemblies over a large area. Here, we demonstrate that high-quality PSi hybrid

Received: June 24, 2014
Published: October 21, 2014

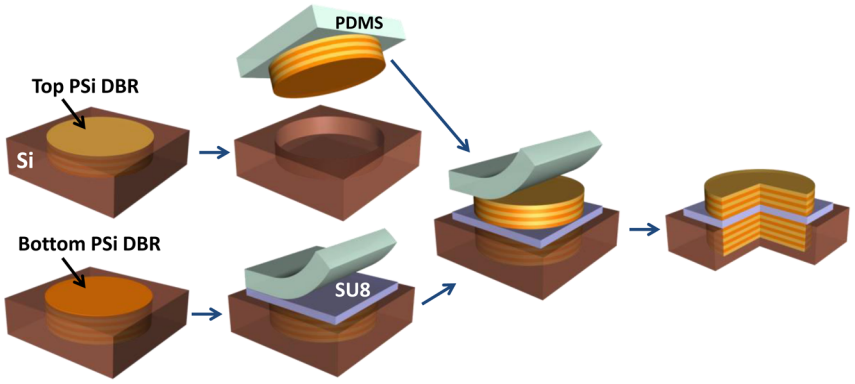

Figure 1. Schematic illustrating the general process flow for the assembly of PSi-based hybrid microcavities. The process features sequential printings of an SU-8 photoresist and a free-standing PSi DBR atop an as-fabricated PSi DBR. The result is a PSi/polymer hybrid microcavity with the cross-sectional structure depicted at the right.

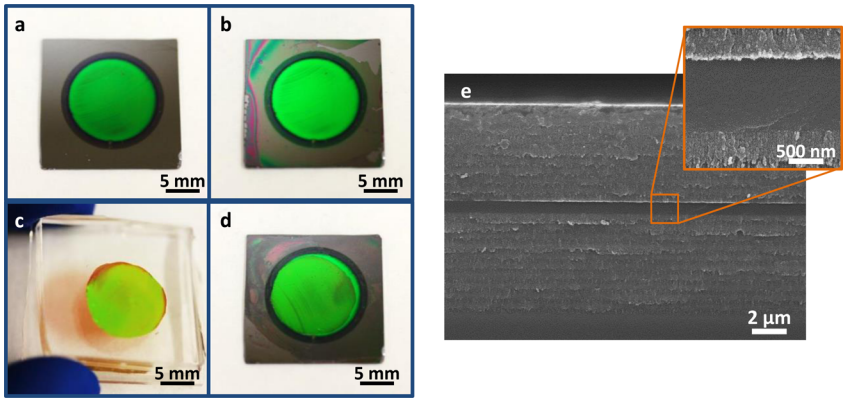

Figure 2. (a–d) Optical micrographs displaying the top view of the PSi/polymer hybrid microcavity at different stages of the assembly process shown in Figure 1 including (a) the as-fabricated PSi DBR (green region), (b) after printing an SU-8 polymer film atop the PSi DBR and the surrounding Si substrate, (c) after picking up a detached PSi DBR with a silane-treated PDMS stamp, and (d) the final PSi/polymer/PSi sandwich structure. (e) Scanning electron microscope (SEM) image of a cross-section of the final PSi/polymer hybrid structure; (inset) higher magnification SEM image focusing on the cavity layer showing the high quality of the interfaces.

microcavities can easily be constructed using a modified transfer-printing technique, enabling strongly controlled emission from any variety of emitters, from quantum dots to solid-state thin films. By introducing a PSi cavity coupling layer in addition to the PSi DBR mirrors, the hybrid microcavity resonance can be both globally tuned and spatially modulated.

RESULTS AND DISCUSSION

Printing Hybrid Porous Silicon Microcavities. Transfer-printing assembly is a pick-and-place method that uses an elastomeric stamp, commonly polydimethylsiloxane (PDMS), as the carrier element.[35] Our initial efforts to transfer-print free-standing PSi were unsuccessful due to the strong adhesion of PSi to the PDMS stamp, making damage-free transfer of the PSi film to a new substrate in an optically flat, planar configuration difficult. The adhesion strength was decreased by a standard silanization procedure[38,39] to the surface of the PDMS stamp. The treated stamp still offers sufficient viscoelasticity[35] to enable successful retrieval and printing of a free-standing PSi DBR film (Figure 1).

A $\lambda/2$ PSi-based hybrid microcavity was constructed by assembling a PSi/polymer hybrid (Figure 1). The polymer, an ~500 nm thick SU-8 photoresist film, was printed onto a PSi DBR consisting of 15 pairs of alternating high (~2.4) and low (~1.7) refractive index layers (Figure 2a,b). Next, another PSi DBR with the same index contrast, but only 11 lattice periods, and thus slightly lower in reflectivity, is transfer-printed onto the SU-8 cavity layer (Figure 2c,d). Figure 2e displays a cross-section of such a hybrid microcavity, showing that the printed SU-8 layer forms smooth, distinct interfaces with the PSi.

The hybrid microcavity is characterized by its reflectance spectrum (Figure 3a), and a sharp (average full-width at half-maximum (fwhm) = 2.1 nm) cavity mode near the center (1500 nm) of the 300 nm wide DBR stop band is observed. Compared to a monolithically etched PSi microcavity with a similar refractive index profile (Figure 3b), the cavity mode of the printed microcavity is only 0.3 nm wider. The small broadening in the line width relative to the monolithic structure is perhaps caused by thickness variations of the SU-8 cavity layer over the measurement spot. Figure 3c shows the measured cavity mode and mode line width across a 9 mm line of the printed SU-8 cavity. The small deviations in mode position (~6.8 nm) and line width (~0.3 nm) demonstrate the ability of this method to assemble large-area, high-quality microcavities.

Incorporating External Emitters. The high optical quality of the hybrid microcavity makes it a strong candidate for controlling the emission of a light emitter. The polymer cavity can serve as a host to any emitters that can be dispersed in a polymer matrix (e.g., organic dye molecules, colloidal quantum

dx.doi.org/10.1021/ph500230j | ACS Photonics 2014, 1, 1144–1150

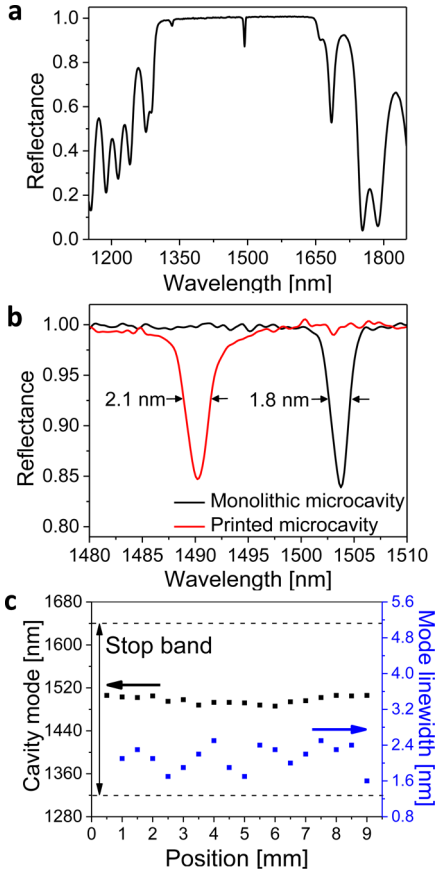

Figure 3. (a) Optical reflectance spectrum of the PSi/polymer hybrid microcavity exhibiting a sharp dip in the middle of the DBR stop band around 1500 nm, confirming the presence of the cavity mode. (b) Comparison of the resonant cavity mode of the printed microcavity with a monolithic PSi microcavity showing the similar optical response of the printed and monolithic devices. (c) Position and line width of the cavity mode at different positions across the sample. The variation in the spectral position and line width of the cavity mode are only ∼6.8 and ∼0.3 nm, respectively.

dots, and rare earth nanocrystals).[40,41] As an example, a PSi/polymer microcavity is formed with PbS quantum dots (QDs) dispersed in the SU-8 cavity layer (Figure 4a). The microcavity resonance (Supporting Figure S1) strongly influences the original, broad emission (fwhm ∼100 nm) of the embedded PbS QDs (Figure 4b), significantly redistributing the emission spectrum in the normal direction to a ∼2.1 nm fwhm at 1198 nm (Supporting Figure S1). This assembly method clearly permits the construction of high-quality structures containing spatially localized emitters in a specifically controlled chemical environment. Because formation of the emitter layer is decoupled from the assembly process, the emitters can be dispersed in a preferred matrix for controlling the physical dispersion to avoid undesirable energy transfer processes that lead to fluorescence quenching.[27−29]

Another major attribute of printing-based assembly is the ease of incorporating a solid-state thin film emitter, such as a group III−V compound semiconductor. Although promising hybrid light-emitting devices consisting of Si and group III−V semiconductors have been demonstrated,[36,42−44] they primarily operate below the Si band gap (λ > 1100 nm) to reduce the absorption loss from Si. The use of PSi can broaden the spectral range of operation, as it exhibits considerably less absorption

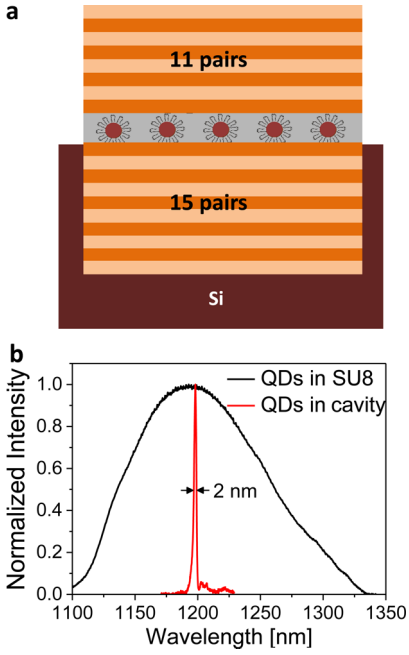

Figure 4. (a) Schematic of a transfer-printed PSi microcavity containing an SU-8 cavity layer doped with PbS QDs. (b) Emission of SU-8 doped with PbS QDs within a hybrid cavity compared to a bare, QD-doped SU-8 film.

above the Si band gap due to the reduced absorbing volume and the increased effective electronic band gap.[45] For example, the calculated absorption losses in the top 11-pair DBR at 870, 900, and 980 nm are only 1.5%, 1.2%, and 0.4%, respectively (Supporting Information). Here, we provide a demonstration of a PSi/III−V hybrid microcavity light-emitting module that operates at energies above the Si band gap. Figure 5a illustrates the structural layout of a hybrid microcavity featuring an ∼1200 nm thick heterogeneous GaAs film. The interfacial SU-8 layers in the structure ensure the complete printing of both the GaAs

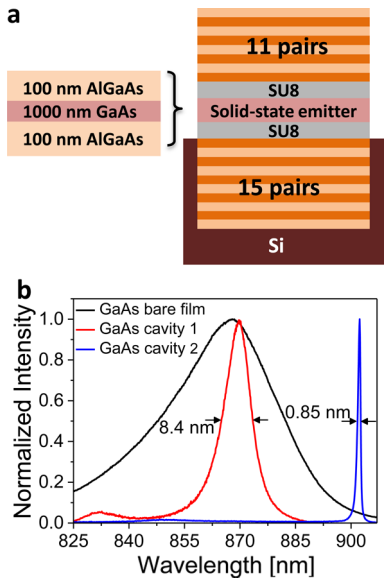

Figure 5. (a) Schematic of transfer-printed PSi/GaAs hybrid emitting structure. (b) Emission data from the bare GaAs structure and the GaAs structure after incorporation in two different cavities, showing a clear modification of the emission of the GaAs by the microcavity.

dx.doi.org/10.1021/ph500230j | ACS Photonics 2014, 1, 1144−1150

layer and the top PSi DBR (Supporting Figure S2), allow control over the total cavity length, and provide extra optical confinement in the emitting layer due to their high refractive index contrast with respect to GaAs. Figure 5b compares the emission spectrum of bare GaAs with those from two separate hybrid microcavities possessing different cavity lengths. The first microcavity's emission peak is near the center of the GaAs emission spectrum (fwhm ~30 nm) and features an 8.4 nm fwhm at 870 nm. The second microcavity structure is constructed with a larger SU-8 thickness that shifts the microcavity resonance to the tail of the GaAs emission spectrum. This leads to a strongly modified emission with a 0.85 nm fwhm at 902 nm (Supporting Figure S3), corresponding to a *Q*-factor ($Q = \lambda_0/\Delta\lambda$) of 1058. Assuming no absorption in the cavity layer, the calculated mode line widths of the two microcavities are 0.7 nm (first) and 0.5 nm (second), respectively, suggesting that the broader line width of the first microcavity is likely dominated by the reabsorption of emitted photons within the GaAs layer at 870 nm and not a result of the printing process or absorption by the PSi DBRs.

Microcavity Resonance Tuning. The ease with which the effective refractive index of PSi can be modulated not only enables the formation of microcavity structures but also provides a simple route to cavity tuning.[22,23] To add tuning to a nonporous polymer or a solid-state cavity layer, the top and bottom DBRs are modified by introducing an additional, monolithic PSi layer above and below the cavity layer. We term this layer the cavity coupling layer (CCL), as it couples with the cavity layer to produce a resonant mode spectrally positioned at $m\lambda = n_1d_1 + n_2d_2 + n_3d_3$, where m is a half-integer multiple, representing the order of the cavity mode, and n_id_i is the optical thickness of the ith layer. The CCL provides a facile route to tune the resonant mode of the assembled hybrid microcavity through gradual infiltration of its mesoporous structure with a conformal deposition tool such as atomic layer deposition (ALD). Figure 6a illustrates a 2λ microcavity consisting of two CCLs and an SU-8 layer doped with PbS QDs. Al_2O_3 is deposited into the top half of the structure at 1.2 Å per ALD cycle (the solid emitter layer blocks deposition of Al_2O_3 into the bottom half of the structure). The Al_2O_3 deposition gradually increases the CCL optical thickness, causing the position of the emission peak to red-shift ~0.9 nm per cycle from its initial position at 1145 nm. The peak eventually settles around 1163 nm after 20 cycles (Figure 6b), suggesting that the mesoporous network has undergone pinch-off.[46] Al_2O_3 infiltration of a simple 15-period DBR structure confirms that the stopband shift does not occur at the expense of the DBR photonic strength (Supporting Figure S4), and thus Al_2O_3 infiltration does not broaden or diminish the strength of the resonant mode of a microcavity structure.

The magnitude of this spectral shifting is linearly proportional to the product of the optical thickness fraction of CCL (i.e., CCL optical thickness relative to total cavity optical thickness) and the refractive index of the material introduced during ALD. Using a three-component effective medium model it is determined that, at pinch-off of the microcavity structure, the CCL is composed of 14% Al_2O_3 by volume (Supporting Information). This corresponds to a change in the effective refractive index of the CCL from ~1.7 to ~1.83. A larger tuning range could be attained either by increasing the CCL fraction (currently the top CCL accounts for 18% of the total cavity optical thickness) or by infiltrating the CCL with higher refractive index materials such as HfO_2, TiO_2, or Si (Supporting Figure S5). While techniques such as ALD permanently shift the cavity mode, reversible tuning based on dynamic control of the infiltration may be possible. Reversible shifts in the optical response of PSi films have, for example, already been demonstrated by infiltration with various solvent vapors.[47,48]

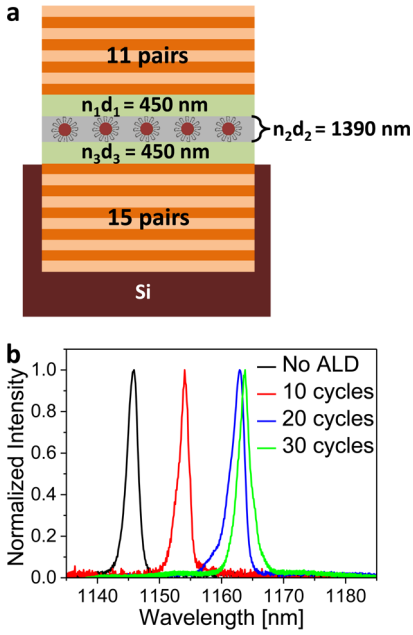

Figure 6. (a) Schematic of a hybrid microcavity containing a CCL (green) and a PbS QD-doped SU-8 layer (gray with red circles). (b) Al_2O_3 ALD is used to gradually increase the optical thickness of the PSi CCL, globally red-shifting the emission of the hybrid cavity until the porous network is pinched off (~20 ALD cycles).

The microcavity resonance can be spatially modulated by using a CCL with a gradient optical thickness (GROT), providing spatial variation of the cavity mode. Because both the refractive index and formation rate of PSi are determined by the local current density,[49] a simple GROT CCL can be produced by a spatially varying current density that is introduced through the electrode configuration used to form the CCL.[50] Here, a Pt ring electrode that resides ~25 mm from the sample is first used to generate a uniform current density distribution during the formation of the PSi DBR. This electrode is then replaced by a Pt wire ~1 mm above the sample, giving rise to a strong radial variation in the current density that produces the GROT CCL. In this design, the PSi DBR and the GROT CCL form a continuous, monolithic structure. Figure 7a is the optical image of one such monolithic structure prior to PSi microcavity assembly. The optical thickness variation is apparent from the CCL side, as visually manifested by the interference fringes. We note that the DBR should be electrochemically etched before the GROT CCL is etched, because the spatially nonuniform formation of the GROT CCL will result in a nonuniform DBR.

A microcavity with symmetric GROT CCLs is fabricated on a glass substrate via double-printing (Supporting Information) and consists of a top DBR (11 pairs) with a GROT CCL component, a 500 nm thick SU-8 layer, and a bottom DBR (15 pairs) with a GROT CCL component (Figure 7b, inset). Figure 7b shows the spatial distribution of the cavity mode across the entire sample. The two GROT CCLs have identical, radially varying optical thickness profiles and, together with the SU-8 layer, produce a $3\lambda/2$ microcavity at the center of the sample. The spatial resonance modulation is designed so that the

dx.doi.org/10.1021/ph500230j | ACS Photonics 2014, 1, 1144−1150

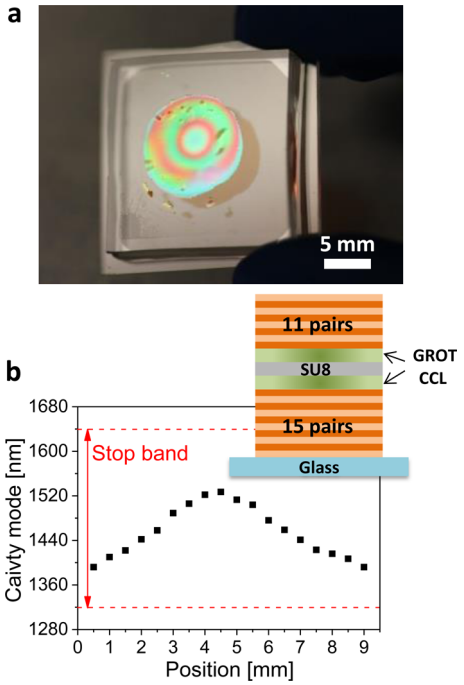

Figure 7. (a) Optical image of a PSi CCL formed with a GROT to spatially modulate the cavity resonance. The GROT is apparent from the appearance of the radially symmetric fringes seen from a GROT-containing PSi CCL and underlying PSi DBR that has been retrieved with a PDMS stamp for printing. (b) Optical response of a GROT PSi CCL in a cavity configuration showing spatial modulation of the spectral position of the cavity resonance by ~140 nm. A schematic of the structure is shown in the inset.

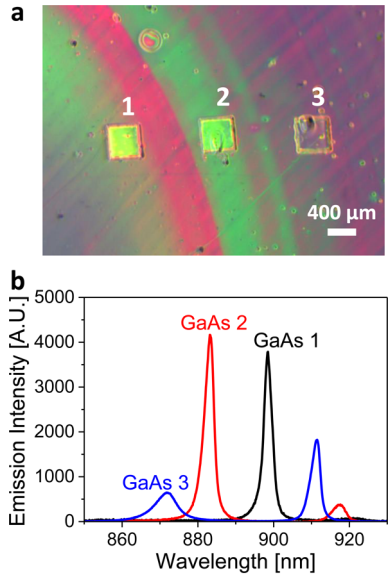

Figure 8. (a) Optical image of a GROT PSi CCL structure containing three distinct GaAs emitter modules. (b) The GROT CCL spatially modulates the emission modification, resulting in spectrally distinct emission from each module.

optical thickness of the microcavity decreases when moving away from the center, eventually blue-shifting the cavity mode ~140 nm from the center to the edge.

An interesting aspect of a GROT CCL is the possibility for introducing different solid-state emitters specifically designed for the local microcavity resonance where they are placed. As a simple demonstration, three separate GaAs thin film emitters are printed ~1 mm apart (Figure 8a) in a microcavity containing a GROT CCL. The emission is collected at the center of each module, which shows that the GROT CCL blue-shifts the modified emission peaks as the total cavity optical thickness decreases from module 1 to module 3 (Figure 8b).

CONCLUSION

We have demonstrated that a modified transfer-printing technique enables the formation of high-quality, PSi-based hybrid microcavities compatible with several classes of light emitters. The versatility of this assembly method was demonstrated by applying it to a hybrid structure of PSi DBRs containing a PbS QD-doped polymer cavity and a PSi/III–V hybrid microcavity light-emitting module operating at energies above the band gap of bulk Si. Using a properly designed gain medium, such as a III–V multiquantum-well structure,[36] we speculate that it may even be possible to realize coherent light sources in the 900–1100 nm wavelength regime using PSi hybrid microcavities. Using a PSi CCL, PSi's inherent index modulation capabilities provided a mechanism for manipulating the hybrid microcavity's resonant cavity mode and emission spectrum. Global tuning of the emission of a hybrid microcavity containing PbS QDs over a spectral range of 18 nm was possible by using Al_2O_3 ALD to infiltrate and thus change the effective optical thickness of the homogeneous CCL. The conformal, atomic-scale infiltration also offers a powerful knob to finely control the spectral shift of the resonant mode. Spatial porosity variations in the form of a GROT CCL enabled spatial resonance modulation generating three emission peaks at distinct spectral positions from each of three GaAs emitter modules located at distinct spatial positions in the hybrid microcavity. The generality of the transfer-printing method, coupled with the unique optical properties of PSi, may offer a new paradigm in the assembly of Si-based photonic architectures for optoelectronic and energy-harvesting applications.

METHODS

PSi Fabrication. The PSi DBR was formed from double-side polished, highly doped (ρ ~0.01–0.03 Ω cm) p-type Si (University Wafers). Etching was carried out in a polypropylene cell with an exposed etch area of ~1.20 cm^2. Contact to the back of the Si was established with a stainless steel electrode. Current was delivered to the cell by an SP-200 research grade potentiostat/galvanostat (Bio-Logic Science Instruments) and pulsed with a duty cycle of 33% at a frequency of 1.33 Hz (unless specified otherwise). The high (low) refractive index layer was formed using a current density of 50 (250) mA cm^{-2}, with the applied etching time varied to achieve the appropriate layer optical thickness for the designed stop band position. After etching, all samples were sequentially rinsed with ethanol and hexanes. The electrolyte comprised a 1:1 volume ratio of 48% hydrofluoric acid(aq) (Sigma-Aldrich) and 100% ethanol (Decon Laboratories). A 5 mm diameter Pt–Ir inoculating loop (Thomas Scientific) served as the counter electrode and was located at the center of the cell ~25 mm from the etch surface to provide a uniform current density across the sample.

The radial GROT CCLs were formed using an electrolyte comprising a 1:3 volume ratio of 48% hydrofluoric acid(aq) and 100% ethanol. A current density of 15 mA cm^{-2} was applied,

dx.doi.org/10.1021/ph500230j | ACS Photonics 2014, 1, 1144–1150

with the Pt−Ir pin electrode placed ∼1 mm from the etch surface.

Electropolishing was carried out with an electrolyte comprising a 1:3 volume ratio of 48% hydrofluoric acid(aq) and 100% ethanol. The 5 mm Pt−Ir ring served as the counter electrode, and a current density of 300 mA cm^{-2} was applied with a duty cycle of 20% at a frequency of 0.40 Hz. Before the electrochemically induced detachment, a stainless steel syringe needle was used to mechanically score and release the edges of the PSi film to allow the film to remain flat for printing. After the electropolishing process, all samples were sequentially rinsed with ethanol and hexanes in a gentle fashion in order to avoid causing the film to be displaced on the Si substrate. Rinsing was followed by drying on a hot plate at 60 °C.

Transfer-Printing. PDMS stamps (Dow-Sylgard 184) were cast onto flat substrates and cut to dimensions 2.5 cm × 2.5 cm × 5 mm. To transfer the SU-8 film, the stamp was treated with oxygen plasma (600 mTorr, 50 W, 80 s) and subsequently spin-coated with SU-8 2000.5 (MicroChem Corp.) at 2000 rpm for 30 s. The SU-8-PDMS stamp was prebaked in a conventional oven at 65 °C for 5 min and then laminated against the receiver substrate (PSi or GaAs). To facilitate the release of the SU-8 layer, both the PDMS and the receiver substrate were heated at 65 °C for 20 min, followed by slow removal of the stamp. To transfer the PSi DBR, the PDMS stamp was treated with oxygen plasma and then exposed to a fluorinated silane vapor for 1 h. The stamp was laminated against the lifted-off PSi film and rapidly peeled away from the donor substrate. The PSi film was subsequently printed onto the receiver substrate (SU-8 film) following the above printing procedure.

QD/SU-8 Composite. PbS core QDs (10 mg mL^{-1} in hexane) were purchased from Evident Technologies. A 0.2 mL amount of the QD solution was slowly added to 0.75 g of a 2000.5 SU-8 solution. The resulting solution was subsequently spin-casted onto an oxygen plasma-treated PDMS stamp at 2000 rpm for 30 s. The composite layer was prebaked at 65 °C for 5 min and finally printed onto the PSi substrate following the procedure described previously.

GaAs Thin Films. An AlGaAs/GaAs/AlGaAs double heterostructure (DH)[51] was formed by growth on a gallium arsenide (GaAs) substrate via metal−organic chemical vapor deposition (MOCVD). The detailed structure (from bottom to top) included the GaAs substrate, a 500 nm $Al_{0.95}Ga_{0.05}As$ sacrificial layer, a 5 nm GaAs protection layer, a 100 nm n-$Al_{0.3}Ga_{0.7}As$ ($n = 3 \times 10^{18}$ cm^{-3}) layer, a 1000 nm p-GaAs ($p = 5 \times 10^{17}$ cm^{-3}) layer, a 100 nm p-$Al_{0.3}Ga_{0.7}As$ ($p = 3 \times 10^{18}$ cm^{-3}) layer, and another 5 nm GaAs protection layer. Zn and Si served as p-type and n-type dopants, respectively. The DH devices (size 400 μm × 400 μm) were lithographically fabricated, using H_3PO_4 (85 wt % in water)/H_2O_2 (30 wt % in water)/H_2O (3:1:25) to etch the GaAs and $Al_{0.3}Ga_{0.7}As$ layers. After removing the $Al_{0.95}Ga_{0.05}As$ sacrificial layer in an ethanol-rich hydrofluoric acid (HF) solution (ethanol/HF = 1.5:1 by volume), individual DH devices were released from the GaAs wafer and then bonded onto PSi DBR by transfer-printing with a flat PDMS stamp.[52] A layer of 500 nm SU-8 acted as an adhesive to facilitate printing.

Optical Characterization. The reflectance spectrum was collected by a Bruker 70 FTIR system with a 4× objective and 1.8 mm aperture at the image plane, corresponding to a 200 μm field of view. Both PbS QDs and the GaAs thin films were excited by a 785 nm continuous wave laser diode. The emission of PbS QDs was recorded by a homemade system with a 4× objective and a NIR CCD detector (Horiba, Symphony). The emission of GaAs was measured by a Horiba confocal Raman imaging microscope with a 4× objective and a 200 μm aperture.

■ ASSOCIATED CONTENT

Ⓢ Supporting Information

High-resolution emission peaks for PbS quantum dot emitter and GaAs emitter microcavity samples, as well as optical micrographs of a single GaAs emitting module and a double-printed, symmetric PSi microcavity with GROT CCLs. Detailed calculations of silicon-based absorption losses in the PSi DBR, the Al_2O_3 content of the CCL used for global tuning, and the double-printing procedure for symmetric PSi microcavities with GROT CCLs. This material is available free of charge via the Internet at http://pubs.acs.org.

■ AUTHOR INFORMATION

Corresponding Author

*E-mail: pbraun@illinois.edu.

Author Contributions

⊥H. Ning and N. A. Krueger contributed equally to this work.

Notes

The authors declare no competing financial interest.

■ ACKNOWLEDGMENTS

This work was supported by the U.S. Department of Energy "Light Material Interactions in Energy Conversion" Energy Frontier Research Center under grant DE-SC0001293 (optical measurements and device assembly) and the Dow Chemical Company (porous silicon etching). This research was also conducted with Government support under and awarded by DoD, Air Force Office of Scientific Research, National Defense Science and Engineering Graduate (NDSEG) Fellowship, 32 CFR 168a (N.A.K.). This research was carried out in part in the Center for Microanalysis of Materials, UIUC, which is partially supported by the U.S. Department of Energy under grants DE-FG02-07ER46453 and DE-FG02-07ER46471. We acknowledge Prof. Kris Kilian and Tiffany Huang for useful discussions regarding PSi fabrication.

■ REFERENCES

(1) Gal, M.; Reece, P. J.; Zheng, W.; Lerondel, G. Porous Silicon: A Versatile Optical Material. *Proc. SPIE* **2004**, *5277*, 9−16.

(2) Canham, L. T. Silicon Quantum Wire Array Fabrication by Electrochemical and Chemical Dissolution of Wafers. *Appl. Phys. Lett.* **1990**, *57*, 1046−1048.

(3) Cullis, A. G.; Canham, L. T. Visible Light Emission Due to Quantum Size Effects in Highly Porous Crystalline Silicon. *Nature* **1991**, *353*, 335−338.

(4) Canham, L. Gaining Light from Silicon. *Nature* **2000**, *408*, 411−412.

(5) Collins, R. T.; Fauchet, P. M.; Tischler, M. A. Porous Silicon: From Luminescence to LEDs. *Phys. Today* **2008**, *50*, 24−31.

(6) Korotcenkov, G.; Cho, B. K. Porous Semiconductors: Advanced Material for Gas Sensor Applications. *Crit. Rev. Solid State Mater. Sci.* **2010**, *35*, 1−37.

(7) Rong, G.; Najmaie, A.; Sipe, J. E.; Weiss, S. M. Nanoscale Porous Silicon Waveguide for Label-Free DNA Sensing. *Biosens. Bioelectron.* **2008**, *23*, 1572−1576.

(8) Rong, G.; Ryckman, J. D.; Mernaugh, R. L.; Weiss, S. M. Label-Free Porous Silicon Membrane Waveguide for DNA Sensing. *Appl. Phys. Lett.* **2008**, *93*, 161109.

(9) Anderson, M. A.; Tinsley-Bown, A.; Allcock, P.; Perkins, E. A.; Snow, P.; Hollings, M.; Smith, R. G.; Reeves, C.; Squirrell, D. J.;

Nicklin, S.; Cox, T. I. Sensitivity of the Optical Properties of Porous Silicon Layers to the Refractive Index of Liquid in the Pores. *Phys. Status Solidi A* **2003**, *197*, 528−533.
(10) Chan, S.; Fauchet, P. M.; Li, Y.; Rothberg, L. J.; Miller, B. L. Porous Silicon Microcavities for Biosensing Applications. *Phys. Status Solidi A* **2000**, *182*, 541−546.
(11) Mulloni, V.; Pavesi, L. Porous Silicon Microcavities as Optical Chemical Sensors. *Appl. Phys. Lett.* **2000**, *76*, 2523−2525.
(12) Frohnhoff, S.; Berger, M. G. Porous Silicon Superlattices. *Adv. Mater.* **1994**, *6*, 963−965.
(13) Ghulinyan, M.; Oton, C. J.; Bonetti, G.; Gaburro, Z.; Pavesi, L. Free-Standing Porous Silicon Single and Multiple Optical Cavities. *J. Appl. Phys.* **2003**, *93*, 9724−9729.
(14) Reece, P. J.; Lérondel, G.; Zheng, W. H.; Gal, M. Optical Microcavities with Subnanometer Linewidths Based on Porous Silicon. *Appl. Phys. Lett.* **2002**, *81*, 4895−4897.
(15) Zheng, W. H.; Reece, P.; Sun, B. Q.; Gal, M. Broadband Laser Mirrors Made from Porous Silicon. *Appl. Phys. Lett.* **2004**, *84*, 3519−3521.
(16) Yablonovitch, E. Inhibited Spontaneous Emission in Solid-State Physics and Electronics. *Phys. Rev. Lett.* **1987**, *58*, 2059−2062.
(17) Schubert, E. F.; Kim, J. K. Solid-State Light Sources Getting Smart. *Science* **2005**, *308*, 1274−1278.
(18) Khitrova, G.; Gibbs, H. M.; Kira, M.; Koch, S. W.; Scherer, A. Vacuum Rabi Splitting in Semiconductors. *Nat. Phys.* **2006**, *2*, 81−90.
(19) Strauf, S. Quantum Optics: Towards Efficient Quantum Sources. *Nat. Photonics* **2010**, *4*, 132−134.
(20) Venturello, A.; Ricciardi, C.; Giorgis, F.; Strola, S.; Salvador, G. P.; Garrone, E.; Geobaldo, F. Controlled Light Emission from Dye-Impregnated Porous Silicon Microcavities. *J. Non-Cryst. Solids* **2006**, *352*, 1230−1233.
(21) Dwivedi, V. K.; Pradeesh, K.; Vijaya Prakash, G. Controlled Emission from Dye Saturated Single and Coupled Microcavities. *Appl. Surf. Sci.* **2011**, *257*, 3468−3472.
(22) Qiao, H.; Guan, B.; Böcking, T.; Gal, M.; Gooding, J. J.; Reece, P. J. Optical Properties of II-VI Colloidal Quantum Dot Doped Porous Silicon Microcavities. *Appl. Phys. Lett.* **2010**, *96*, 161106.
(23) Weiss, S. M.; Zhang, J.; Fauchet, P. M.; Seregin, V. V.; Coffer, J. L. Tunable Silicon-Based Light Sources Using Erbium Doped Liquid Crystals. *Appl. Phys. Lett.* **2007**, *90*, 031112.
(24) DeLouise, L. A.; Ouyang, H. Photoinduced Fluorescence Enhancement and Energy Transfer Effects of Quantum Dots Porous Silicon. *Phys. Status Solidi C* **2009**, *6*, 1729−1735.
(25) Jenie, S. N. A.; Pace, S.; Sciacca, B.; Brooks, R. D.; Plush, S. E.; Voelcker, N. H. Lanthanide Luminescence Enhancements in Porous Silicon Resonant Microcavities. *ACS Appl. Mater. Interfaces* **2014**, *6*, 12012−12021.
(26) Reece, P. J.; Gal, M.; Tan, H. H.; Jagadish, C. Optical Properties of Erbium-Implanted Porous Silicon Microcavities. *Appl. Phys. Lett.* **2004**, *85*, 3363−3365.
(27) Tan, M. C.; Kumar, G. A.; Riman, R. E.; Brik, M. G.; Brown, E.; Hommerich, U. Synthesis and Optical Properties of Infrared-Emitting YF3:Nd Nanoparticles. *J. Appl. Phys.* **2009**, *106*, 063118.
(28) Rinnerbauer, V.; Egelhaaf, H.-J.; Hingerl, K.; Zimmer, P.; Werner, S.; Warming, T.; Hoffmann, A.; Kovalenko, M.; Heiss, W.; Hesser, G.; Schaffler, F. Energy Transfer in Close-Packed PbS Nanocrystal Films. *Phys. Rev. B* **2008**, *77*, 085322.
(29) Clegg, R. M. Fluorescence Resonance Energy Transfer. *Curr. Opin. Biotechnol.* **1995**, *6*, 103−110.
(30) Sirbuly, D. J.; Lowman, G. M.; Scott, B.; Stucky, G. D.; Buratto, S. K. Patterned Microstructures of Porous Silicon by Dry-Removal Soft Lithography. *Adv. Mater.* **2003**, *15*, 149−152.
(31) Böcking, T.; Kilian, K. A.; Reece, P. J.; Gaus, K.; Gal, M.; Gooding, J. J. Biofunctionalization of Free-Standing Porous Silicon Films for Self-Assembly of Photonic Devices. *Soft Matter* **2011**, *8*, 360−366.
(32) Böcking, T.; Kilian, K. A.; Reece, P. J.; Gaus, K.; Gal, M.; Gooding, J. J. Substrate Independent Assembly of Optical Structures Guided by Biomolecular Interactions. *ACS Appl. Mater. Interfaces* **2010**, *2*, 3270−3275.
(33) Gargas, D. J.; Muresan, O.; Sirbuly, D. J.; Buratto, S. K. Micropatterned Porous-Silicon Bragg Mirrors by Dry-Removal Soft Lithography. *Adv. Mater.* **2006**, *18*, 3164−3168.
(34) Kim, S.; Wu, J.; Carlson, A.; Jin, S. H.; Kovalsky, A.; Glass, P.; Liu, Z.; Ahmed, N.; Elgan, S. L.; Chen, W.; Ferreira, P. M.; Sitti, M.; Huang, Y.; Rogers, J. A. Microstructured Elastomeric Surfaces with Reversible Adhesion and Examples of Their Use in Deterministic Assembly by Transfer Printing. *Proc. Natl. Acad. Sci. U.S.A.* **2010**, *107*, 17095−17100.
(35) Meitl, M. A.; Zhu, Z.-T.; Kumar, V.; Lee, K. J.; Feng, X.; Huang, Y. Y.; Adesida, I.; Nuzzo, R. G.; Rogers, J. A. Transfer Printing by Kinetic Control of Adhesion to an Elastomeric Stamp. *Nat. Mater.* **2006**, *5*, 33−38.
(36) Yang, H.; Zhao, D.; Chuwongin, S.; Seo, J.-H.; Yang, W.; Shuai, Y.; Berggren, J.; Hammar, M.; Ma, Z.; Zhou, W. Transfer-Printed Stacked Nanomembrane Lasers on Silicon. *Nat. Photonics* **2012**, *6*, 615−620.
(37) Justice, J.; Bower, C.; Meitl, M.; Mooney, M. B.; Gubbins, M. A.; Corbett, B. Wafer-Scale Integration of Group III-V Lasers on Silicon Using Transfer Printing of Epitaxial Layers. *Nat. Photonics* **2012**, *6*, 610−614.
(38) Xia, Y.; Whitesides, G. M. Soft Lithography. *Annu. Rev. Mater. Sci.* **1998**, *28*, 153.
(39) Qin, D.; Xia, Y.; Whitesides, G. M. Soft Lithography for Micro- and Nanoscale Patterning. *Nat. Protoc.* **2010**, *5*, 491−502.
(40) Stouwdam, J. W.; van Veggel, F. C. J. M. Near-Infrared Emission of Redispersible Er^{3+}, Nd^{3+}, and Ho^{3+} Doped LaF_3 Nanoparticles. *Nano Lett.* **2002**, *2*, 733−737.
(41) Ning, H.; Mihi, A.; Geddes, J. B.; Miyake, M.; Braun, P. V. Radiative Lifetime Modification of LaF_3:Nd Nanoparticles Embedded in 3D Silicon Photonic Crystals. *Adv. Mater.* **2012**, *24*, OP153−OP158.
(42) Lee, A.; Liu, H.; Seeds, A. Semiconductor III−V Lasers Monolithically Grown on Si Substrates. *Semicond. Sci. Technol.* **2013**, *28*, 015027.
(43) Park, H.; Fang, A.; Kodama, S.; Bowers, J. Hybrid Silicon Evanescent Laser Fabricated with a Silicon Waveguide and III-V Offset Quantum Wells. *Opt. Express* **2005**, *13*, 9460−9464.
(44) Fang, A. W.; Park, H.; Jones, R.; Cohen, O.; Paniccia, M. J.; Bowers, J. E. A Continuous-Wave Hybrid AlGaInAs-Silicon Evanescent Laser. *IEEE Photonics Technol. Lett.* **2006**, *18*, 1143−1145.
(45) Datta, S.; Narasimhan, K. L. Model for Optical Absorption in Porous Silicon. *Phys. Rev. B* **1999**, *60*, 8246−8252.
(46) Brzezinski, A.; Chen, Y.-C.; Wiltzius, P.; Braun, P. V. Complex Three-Dimensional Conformal Surfaces Formed by Atomic Layer Deposition: Computation and Experimental Verification. *J. Mater. Chem.* **2009**, *19*, 9126−9130.
(47) Bjorklund, R. B.; Zangooie, S.; Arwin, H. Color Changes in Thin Porous Silicon Films Caused by Vapor Exposure. *Appl. Phys. Lett.* **1996**, *69*, 3001−3003.
(48) Bjorklund, R. B.; Zangooie, S.; Arwin, H. Planar Pore-Filling — Adsorption in Porous Silicon. *Adv. Mater.* **1997**, *9*, 1067−1070.
(49) Ilyas, S.; Gal, M. Single and Multi-Array GRIN Lenses from Porous Silicon. In *2006 Conference on Optoelectronic and Microelectronic Materials and Devices*; 2006; pp 245−248.
(50) Collins, B. E.; Dancil, K.-P. S.; Abbi, G.; Sailor, M. J. Determining Protein Size Using an Electrochemically Machined Pore Gradient in Silicon. *Adv. Funct. Mater.* **2002**, *12*, 187−191.
(51) Schnitzer, I.; Yablonovitch, E.; Caneau, C.; Gmitter, T. J. Ultrahigh Spontaneous Emission Quantum Efficiency, 99.7% Internally and 72% Externally, from AlGaAs/GaAs/AlGaAs Double Heterostructures. *Appl. Phys. Lett.* **1993**, *62*, 131−133.
(52) Carlson, A.; Bowen, A. M.; Huang, Y.; Nuzzo, R. G.; Rogers, J. A. Transfer Printing Techniques for Materials Assembly and Micro/Nanodevice Fabrication. *Adv. Mater.* **2012**, *24*, 5284−5318.